Microelectronic Engineering xxx (2013) xxx–xxx

Contents lists available at SciVerse ScienceDirect

Microelectronic Engineering

journal homepage: www.elsevier.com/locate/mee

Effect of GaP and GaP/InGaP insertion layers on the structural and optical properties of InP quantum dots grown by metal-organic vapor phase epitaxy

S.S. Han [a,*], A. Higo [c], W. Yunpeng [b], M. Deura [b], M. Sugiyama [b], Y. Nakano [b,c], S. Panyakeow [a], S. Ratanathammaphan [a,*]

[a] Semiconductor Device Research Laboratory (NanoTec Center of Excellent), Department of Electrical Engineering, Chulalongkorn University, Bangkok 10330, Thailand
[b] Department of Electrical Engineering and Information Systems, School of Engineering, The University of Tokyo, Japan
[c] Research Center for Advanced Science and Technology, The University of Tokyo, Japan

ARTICLE INFO

Article history:
Available online xxxx

Keywords:
InP, GaP
InGaP
Self-assembled quantum dots (SAQDs)
Metal-organic vapor phase epitaxy (MOVPE)
Atomic force microscopy (AFM)
Photoluminescence (PL)

ABSTRACT

A comparison of ultra-thin insertion layers (GaP and GaP/$In_{0.4}Ga_{0.6}P$) on InP self-assembled quantum dots (SAQDs) grown on GaAs (001) substrates using metal-organic vapor phase epitaxy (MOVPE) was studied. Atomic force microscopy (AFM) and photoluminescence (PL) were employed to characterize the optical and structural properties of the grown InP QDs. It is found that the QD dimension, size distribution and density strongly depend on the insertion layer thickness which led to tune the emission wavelength and narrowing of full width at half maximum (FWHM) at low temperature (20–250 K) and at room-temperature PL measurements. This result is attributed to the improved QD size and quantum confinement effect arising from the insertion of the GaP and GaP/$In_{0.4}Ga_{0.6}P$ layers.

1. Introduction

Indium phosphide (InP) has generated much interest in the past decade due to its superior advantages for application in optoelectronic integrated circuits, high speed microwave, and millimeter wave circuits, solar cells, and wireless applications [1–6]. For these purposes, optically or electrically addressable self-assembled QDs would be needed on a mass production scale which favors metal-organic vapor-phase epitaxy (MOVPE) due to several advantages [7,8]. One of the remaining issues in forming QDs is how to increase their effective density. Many researchers have already attempted to create high density QD heterostructures. III-phosphide QD heterostructures have been a promising for visible-light emitting applications because of their larger band gap energies [9]. Although a room-temperature injection laser has been realized in InP QDs devices [10,11], the threshold current densities are still much higher than those reported in the III-arsenide QD system [12]. The main problem is that the size of the InP QDs is not uniform. A bimodal size distribution was observed when growing InP QDs on InGaP matrices [12–14]. By inserting a few monolayer (ML) of GaP between the InP QDs and the InGaP matrix layer, it was found that the critical thickness of the wetting layer increases and the size uniformity is improved [14]. Improvement of size homogeneity of MOCVD InP QDs on $In_{0.48}Ga_{0.52}P$ via growth of an inserted GaP layer has also been reported [15–17] In the case of metal-organic vapor phase epitaxy (MOVPE) growth InP/GaInP SAQDs, bimodal size distribution for the coherent islands can be overcome by using a GaP insertion layer (IL) yet, the island size is still large and the areal dot density is low [18,19]. Since large dots may introduce dislocations and low density leads to poor optical efficiency, growth of small size, high density and uniformity InP dots becomes imperative. In this work, we have an objective to study the effects of inserted GaP and GaP/$In_{0.4}Ga_{0.6}P$ layers on the structural and optical properties of InP QDs grown by metal-organic vapor phase epitaxy (MOVPE). We have grown 2 series of InP QDs samples with GaP (0–4 ML) and GaP (2 ML)/$In_{0.4}Ga_{0.6}P$ (0–4 ML) ILs on $In_{0.48}Ga_{0.52}P$ matrices lattice matched to GaAs. In the theoretical model of the S-K growth mode, QD depends both on the strain and the surface condition of the layer upon which dots are grown. Therefore, insertion of GaP and GaP/$In_{0.4}Ga_{0.6}P$ layers between $In_{0.49}Ga_{0.51}P$ buffer and InP QDs layer is also expected to change the morphology and optical properties of the InP SAQDs.

2. Experimental details

In this study, the growth of quantum dots composed of InP embedded in $In_{0.49}Ga_{0.51}P$ matrix was carried out on nominally (001) oriented GaAs substrate in a horizontal MOVPE reactor (AIXTRON, AIX200/4) with a rotating substrate holder. The reactor has two inlets. Group-III precursors are introduced through the upper inlet and group-V precursors are introduced through the lower

* Corresponding author. Tel.: +66 2 218 6522; fax: +66 2 218 6523.
E-mail addresses: rsomchai@chula.ac.th, ssoehan@gmail.com (S.S. Han).

0167-9317/$ - see front matter © 2013 Elsevier B.V. All rights reserved.
http://dx.doi.org/10.1016/j.mee.2013.01.026

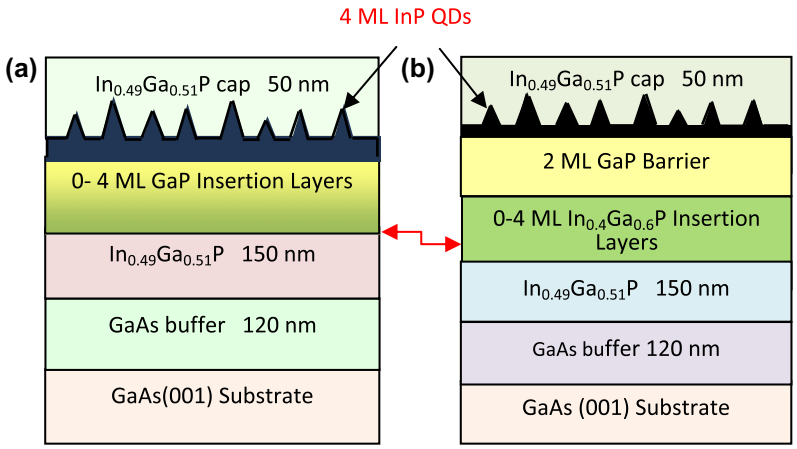

Fig. 1. Schematic diagram of the vertical layer structure of InP QDs grown on (0 0 1) GaAs substrate with (a) GaP insertion layer and (b) GaP/$In_{0.4}Ga_{0.6}P$ insertion layers.

inlet. Hydrogen gas was used as the carrier for precursors and as the coolant between the inner reactor and the outer tube. The reactions occur in a rectangular inner liner tube, which has a graphite rotator as a sample susceptor. During MOVPE growth, GaAs substrates were placed at the center of the susceptor. Trimethylgallium (TMGa) and trimethylindium (TMIn), tertiarybutylarsine (TBAs), and tertiarybutylphosphine (TBP) were used as precursors.

Epitaxial growth conditions were a total pressure of 100 mbar, H_2 total flow rate of 13,000 sccm (cubic centimeter per minute at standard temperature and pressure), temperature of 610 °C, and V/III ratio of source precursors of 18 for InP. 120 nm GaAs buffer layers were first grown on semi-insulating GaAs (0 0 1) substrates at 610 °C. After the growth of GaAs buffer, growth of 150 nm lattice-matched $In_{0.49}Ga_{0.51}P$ layers was followed at the same temperature. Then, a GaP (0–4 ML) insertion layer was deposited. The formation of self-assembled InP QDs was performed at a growth rate of 0.5 ML/s by depositing a 4 ML InP QDs layer. For the photoluminescence (PL) measurement, other samples with 50 nm $In_{0.48}Ga_{0.52}P$ cap layer were grown repeatedly under the same conditions. For GaP IL comparison, a $In_{0.4}Ga_{0.6}P$ (1–4 ML) IL was inserted between GaP and $In_{0.48}Ga_{0.52}P$. All the growth conditions are the same as the GaP IL samples except a 2 ML-thick GaP stabilize layer was sandwiched between the InP QDs and the GaP/$In_{0.4}Ga_{0.6}P$ IL. We examined the morphological and optical properties of InP QDs due to insertion of GaP and GaP/$In_{0.4}Ga_{0.6}P$ ILs by using atomic force microscopy (AFM) and photoluminescence (PL) measurement at room-temperature and at low-temperature (20–250 K). PL measurement was carried out using a 532 nm line of solid state laser and the luminescence signal was collected by an InGaAs photodetector. Temperature dependent PL spectra were measured using a 488 nm line Ar-ion laser. The schematic representation of InP QDs structures are depicted in Fig. 1.

3. Results and discussion

The influence of GaP and GaP/$In_{0.4}Ga_{0.6}P$ ILs on the structural properties of InP SAQDs was investigated by AFM measurement. Fig. 2(a) shows ($1 \times 1\ \mu m^2$) AFM images of InP quantum dots grown with (0–4 ML) GaP and GaP/$In_{0.4}Ga_{0.6}P$ ILs. Histograms of the InP QD diameter are shown in Fig. 2(b). The results show that GaP/$In_{0.4}Ga_{0.6}P$ IL samples have a better uniformity. The average height and diameter of the reference InP QDs (without IL) are 25 nm and 85 nm, respectively. The comparison of diameter, height, and density of InP QDs grown with GaP and $In_{0.4}Ga_{0.6}P$ insertion layers are shown in Fig. 3(a), (b), and (c). We note that the density of the InP QDs increases and the height of the QDs decreases with increasing the GaP and InGaP ILs' thicknesses, which is also consistent with the finding in the literature. Initially, we see that the size of the QDs decreases and the density increases with an increase in the thickness of GaP and $In_{0.4}Ga_{0.6}P$ ILs from 0 to 2 ML. The dot density increases from $2.3 \times 10^9\ cm^{-2}$ to $4.2 \times 10^9\ cm^{-2}$ due to the insertion of 0 ML to 2 ML and decreases from $3.6 \times 10^9\ cm^{-2}$ to $3.3 \times 10^9\ cm^{-2}$ due to the insertion of 3 ML to 4 ML for the GaP IL samples. For GaP/$In_{0.4}Ga_{0.6}P$ samples, the thickness of $In_{0.4}Ga_{0.6}P$ IL is increased from 3 ML to 4 ML, with a slightly increase in density from $3.4 \times 10^9\ cm^{-2}$ to $3.6 \times 10^9\ cm^{-2}$ and an increase in the sizes of QDs. These results verified that the insertion of GaP and GaP/$In_{0.4}Ga_{0.6}P$ ILs had an effect on the size and density of InP QDs. This effect could be effected by the material nucleation step at 2D-3D transition caused by atomic intermixing between the InP QDs and the underlying insertion layers. The difference in nucleation enthalpy between InP QDs – GaP IL and InP QDs – GaP/$In_{0.4}Ga_{0.6}P$ IL is responsible for the difference sized QDs on these ILs. The significantly improved density was achieved at 2 ML GaP IL thickness. It is also shown within the InP QD nucleation effect on ILs. The nuclei centers first increased with an increase in density of QDs due to insertion of GaP thickness from 0 ML to 2 ML, afterwards nucleation was completed and further increased in the thickness did not increase the density of QDs. Through a close examination of the effect of the GaP and GaP/$In_{0.4}Ga_{0.6}P$ ILs on the surface morphology of InP QDs, the latter gives the smaller QD sizes and slightly larger in density due to the strain-induced inter-diffusion process. InP QDs formation must be driven by the total strain field of the system including the strain field due to the lattice-mismatched between InP and ILs. The introduced strain in the lower ILs influences the InP QD growth, in a sense that the same amount of material is deposited but is rearranged into more numbers of smaller QDs. During the inter-diffusion process, In from the $In_{0.4}Ga_{0.6}P$ IL intermixes with Ga from the stabilizing GaP layer and the underlying InGaP layer. Depletion of In in the insertion layer due to the inter-diffusion provides the driving force for diffusive transport of In away from the islands and compensating the In loss of InP QDs due to inter-diffusion. The morphological results obtained from GaP and GaP/$In_{0.4}Ga_{0.6}P$ ILs offer an opportunity to control sizes and densities of QDs, which is essential for applications of QDs to be succeeded. The density and dimension of QDs depends on the thickness and strain effect of insertion layers. However, the density is not high density ($\sim 10^{10}\ cm^{-2}$) due to the low growth rate of QD (0.5 ML/s) in this work. We use a low growth rate to clearly observe the change of morphology and avoid the density saturation effect.

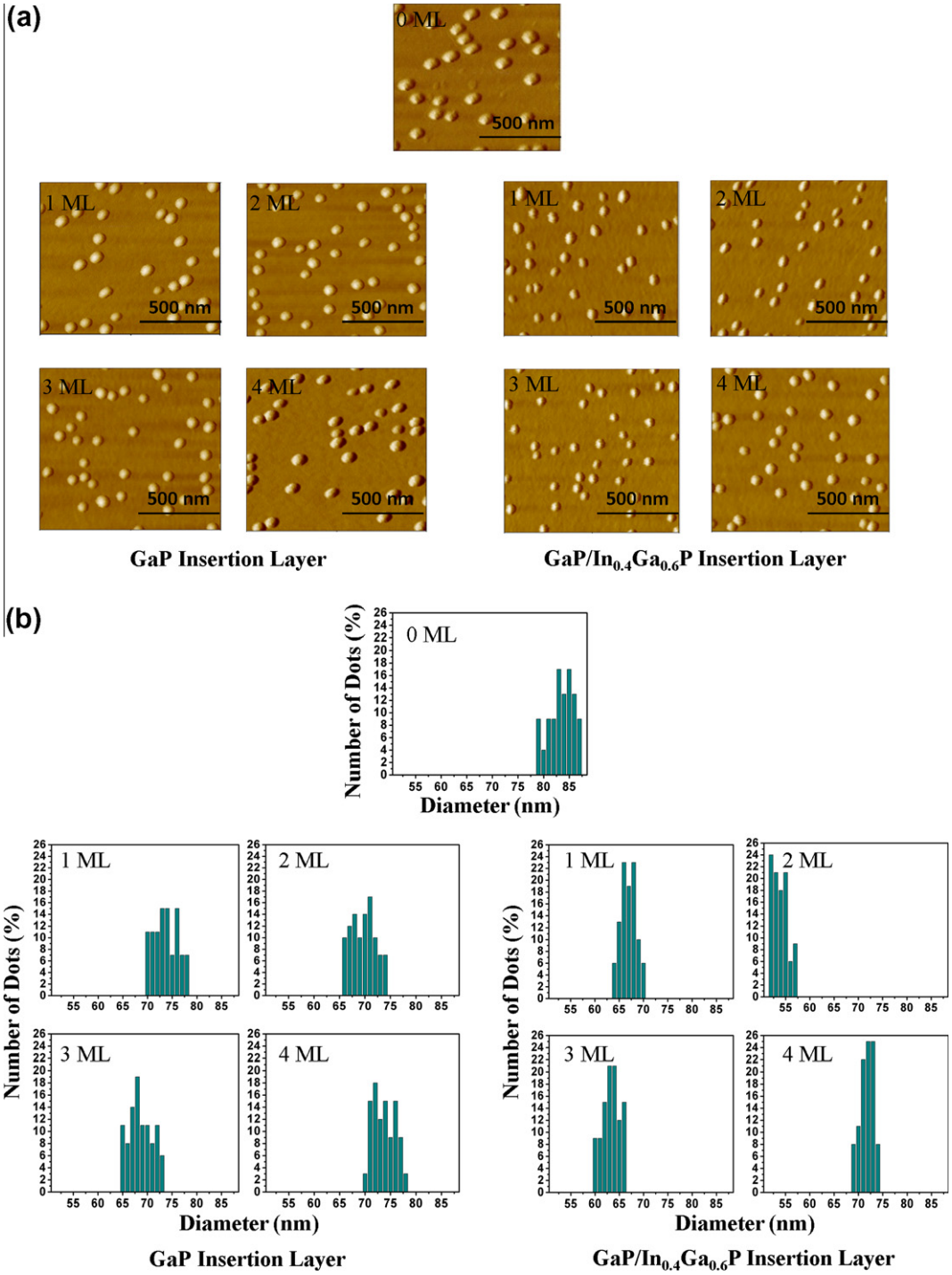

Fig. 2. (a) Typical ($1 \times 1\ \mu m^2$) scan range AFM images of InP QDs with a various thickness of GaP and GaP/$In_{0.4}Ga_{0.6}P$ insertion layers and (b) Diameter distribution histograms of InP QDs for all samples.

In order to further investigate the phenomena related to the effect of GaP and GaP/$In_{0.4}Ga_{0.6}P$ ILs, we have characterized the optical properties by PL measurements at room-temperature and at low-temperature (20–250 K). The low-temperature measurement was performed so that the PL peaks associated with the GaP and GaP/$In_{0.4}Ga_{0.6}P$ ILs were discernible. Meanwhile, the room-temperature measurements were carried out for the fact that practical devices must be able to operate at room-temperature [20]. It is found that PL spectra associated with the GaP and GaP/$In_{0.4}Ga_{0.6}P$ ILs have a narrower FWHM compared with that of the PL spectrum without IL. The results in Fig. 4(a) and (b) show that the FWHM of the PL peaks were measured to be 123 and 84 meV for the samples without and with GaP and GaP/$In_{0.4}Ga_{0.6}P$ ILs, respectively. A narrower FWHM value indicates that the samples with GaP and GaP/$In_{0.4}Ga_{0.6}P$ ILs have an improvement of dot size uniformity than that of the sample without IL. The PL peak of the sample without ILs is at about 1.51 eV while that of the samples with GaP and GaP/$In_{0.4}Ga_{0.6}P$ ILs blueshifted to 1.58 and 1.59 eV because the samples with ILs have smaller dot sizes. The FWHM of the GaP IL samples was similar to that of the InGaP IL samples.

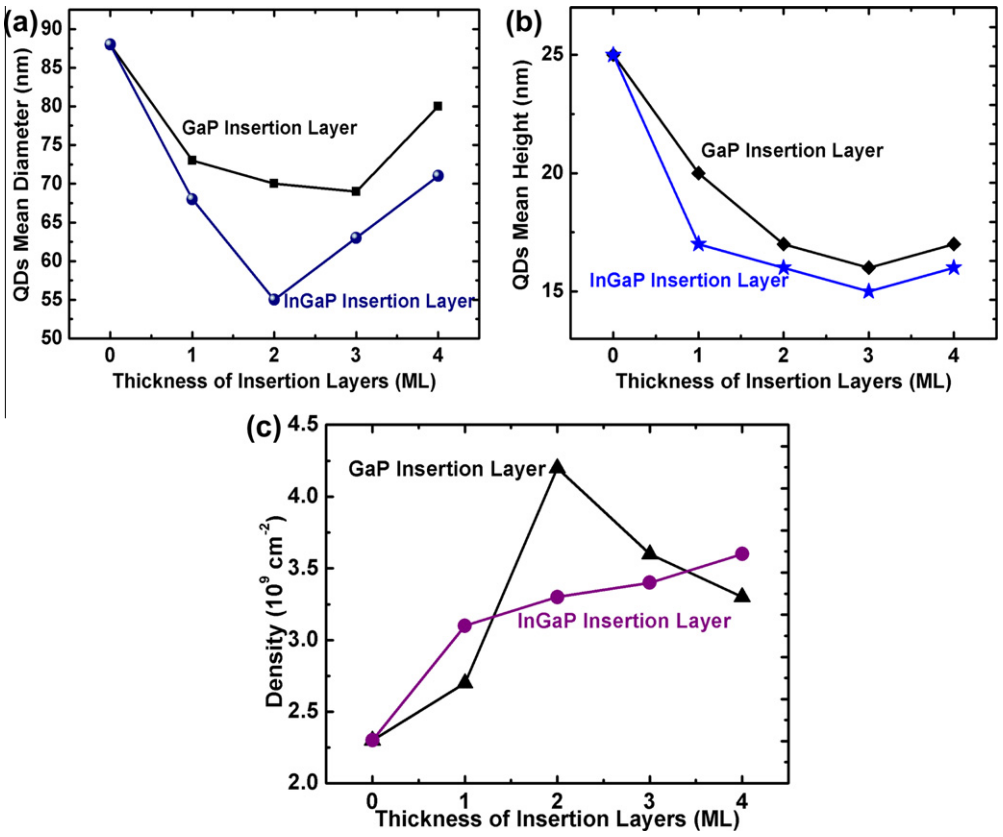

Fig. 3. Effect of GaP and GaP/$In_{0.4}Ga_{0.6}P$ insertion layers on InP SAQDs grown at 610 °C (a) comparison of diameter, (b) comparison of height and (c) comparison of density.

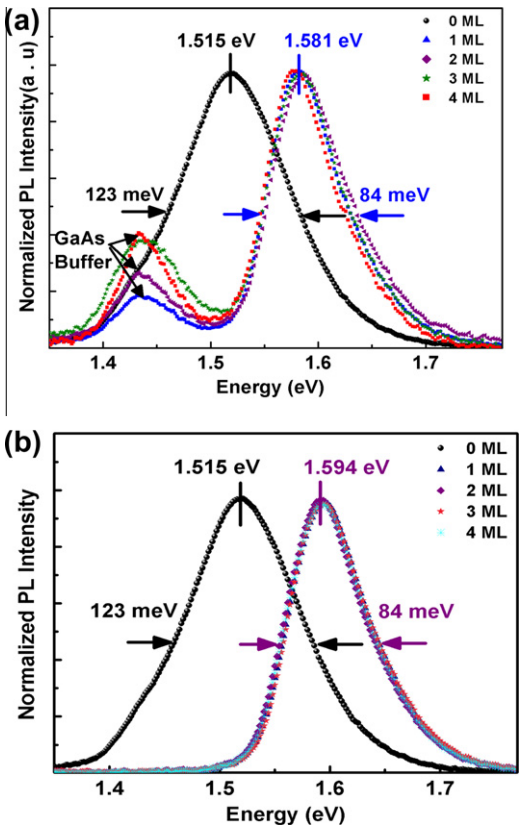

Fig. 4. The room temperature normalized PL spectra of the InP QDs grown on the InGaP barrier with 0–4 ML thick (a) GaP insertion layer and (b) GaP/$In_{0.4}Ga_{0.6}P$ insertion layer.

The presence of GaP and GaP/$In_{0.4}Ga_{0.6}P$ ILs results in better uniformity and smaller QD size, leading to a narrower FWHM and a blueshift of the PL peaks, it might affect optical properties of potential quantum optic devices which have to be carried out in future work. However, the room-temperature measurement was found not to fully describe the role of thickness of these ILs.

To accurately extract more detailed information of these two ILs on the optical properties, we carried out temperature-dependent PL measurement in the 20–250 K range. Figs. 5(a) and (b) show the characterization of PL spectra measured at 77 K with an excitation power of 20 mW. What is particularly noteworthy in Fig. 5(a) is the disappearance of the bimodal size distribution of QDs due to insertion of GaP and GaP/$In_{0.4}Ga_{0.6}P$ ILs. The inset in this figure shows the peak convolution of two peaks due to the bimodal size distribution of QDs. The inset also shows the Gaussian fitting of large (L) and small (S) QDs' PL peaks at 1.57 and 1.62 eV, respectively, indicating that the bimodal size distribution is dominant in no IL sample. Moreover, the blueshift of PL spectra of GaP/$In_{0.4}Ga_{0.6}P$ IL samples, compared with that of GaP ILs, convinces that the smaller QD sizes are obtained. Consequently, the PL peak is greatly blueshifted in additional to the largely FWHM narrowing due to the insertion of GaP and GaP/$In_{0.4}Ga_{0.6}P$ layers, as can be seen in Fig. 5(b). This is confirmed that the QDs size becomes smaller as already described by AFM and the better uniformity. Without the ILs, the PL peak is observed at 1.574 eV and the FWHM is 73 meV. When the 1 ML IL is introduced, the PL peak is blueshifted to 1.636 eV with GaP IL and 1.640 eV with GaP/$In_{0.4}Ga_{0.6}P$ IL, respectively. In case of GaP IL with 2 and 3 ML thickness, the PL peak is continuously blueshifted and then the peak shift is changed to redshift (1.620 eV) at 4 ML. Besides, the PL peak of GaP/$In_{0.4}Ga_{0.6}P$ IL samples is also blueshifted at 2 ML and the shift is changed to redshift 1.638 eV at 3 ML and 1.635 eV at 4 ML, respectively. This PL peak shift coherently reflected the AFM characterization, in

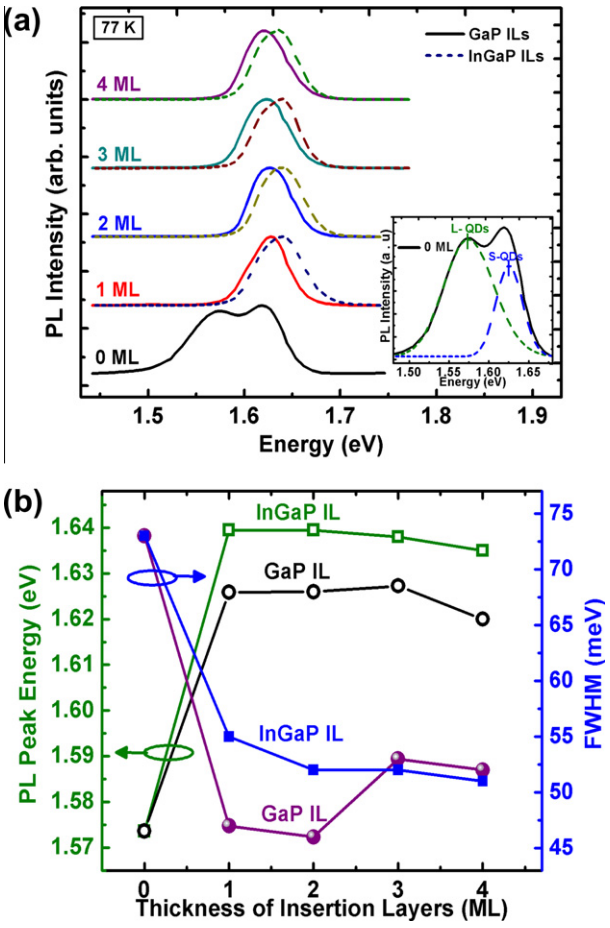

Fig. 5. Comparison of (a) normalized PL spectra from samples with GaP IL (solid lines) and GaP/$In_{0.4}Ga_{0.6}P$ ILs (dashed lines) measured at 77 K. The inset represents the Gaussian fitting of 0 ML IL PL peak with dominant size in large and small QDs (L and S QDs) and (b) the peak position (eV) and FWHM (meV) for samples with ILs.

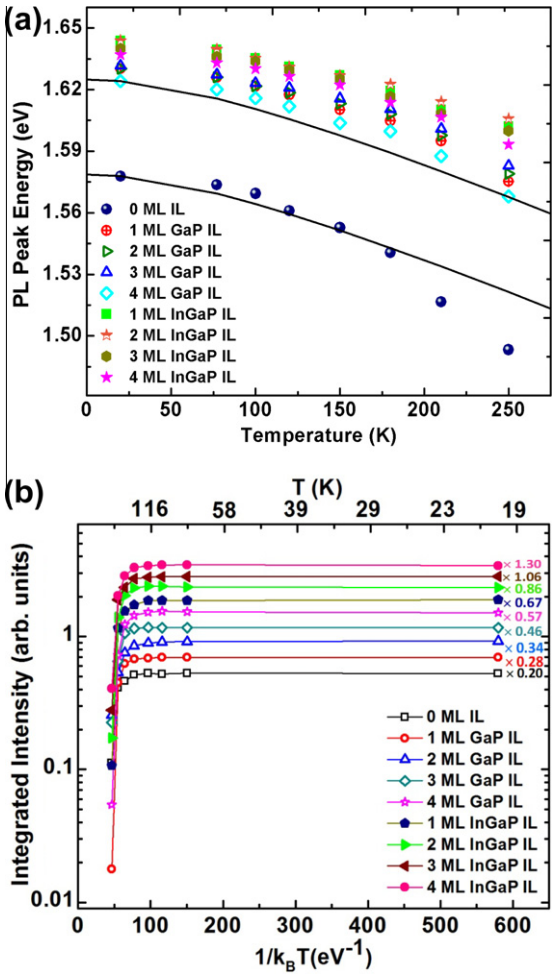

Fig. 6. (a) Temperature dependences of the peak energies of the PL spectra of samples with GaP and InGaP ILs. The continuous lines are calculated according to the Varshni law using the parameters of InP and the peak energies are shifted along the energy axis and (b) The integrated PL intensity as a function of $1/k_BT$ measured from samples with GaP and GaP/$In_{0.4}Ga_{0.6}P$ ILs (each graph was scale up or down to avoid overlapping).

which the PL peak blueshift of the GaP/$In_{0.4}Ga_{0.6}P$ IL was higher in comparison with that of the GaP IL. This phenomenon can be attributed to the reduction of QD size due to In and Ga interdiffusion provides the strain relaxing process between InP and GaP/$In_{0.4}Ga_{0.6}P$ IL. The FWHM of 1 and 2 ML GaP IL samples are narrowly noticeable leading to a better QD uniformity. There was no significant difference between the FWHM of 3 and 4 ML in both ILs' samples. Although the dimension of samples depends on the insertion layer thickness in each condition, the PL peaks at the same temperature are clearly different because of the smaller valence band offset of InP/GaP than that of InP/$In_{0.49}Ga_{0.51}P$ [21].

The transition of PL peak energy as a function of the temperature (20–250 K) is reported, as shown in Fig. 6(a). The figure shows that the peak energies nicely suit the Varshni law with the InP parameters, over the whole temperature range. Consequently, the temperature dependence of the bandgap is confirmed typical for III-V semiconductors. Moreover, the redshift of the PL peak energy in InP bulk is attributed to the electron–phonon scattering owing to the increase of temperature which are frequently observed in a bulk semiconductor [22]. The emission shift is attributed to the thermal excitation [23]. While rising temperature, electrons localized in the small dots are thermally activated to the wetting layer and migrate to larger dots. In the cases of GaP and GaP/$In_{0.4}Ga_{0.6}P$ samples, the energy transition was similar being 55, 51, 48 and 56 meV (for 1, 2, 3 and 4 ML GaP ILs) and 41, 37, 40 and 43 meV (for 1, 2, 3 and 4 ML InGaP ILs), respectively, at temperature range from 20 to 250 K. However, the change of the peak energy with temperature in the case of 0 ML IL was about 84 meV at the same temperature range. This result could be explained by the fact that the activation is quite different for the dots of different size. The QD with lower activation energy should be excited less at the same temperature. This results in the redshift of the PL peak and the decrease of the PL intensity due to the activation mechanism. Fig. 6(b) is the integrated intensity as a function of $1/k_BT$ on the temperature dependency taken from two series of samples. The intensity follows the equation [22]:

$$I = C\exp(E_a/k_BT), \tag{1}$$

where I is the integrated intensity, C is a constant, E_a is the activation energy, and k_B is the Boltzmann constant. The activation energies obtain through Eq. (1) are 64.9 meV (0 ML), 67.7, 71.9, 69.4, and 70.3 meV (for 1, 2, 3, and 4 ML GaP ILs) and 71.4, 78.4, 69.5, and 71.9 meV (for 1, 2, 3,and 4 ML InGaP ILs). As a result, there was no significant difference in the activation energies in spite of the thickness difference of the GaP and GaP/$In_{0.4}Ga_{0.6}P$ ILs. This means that the exciton in the grown InP QDs is strongly localized at a certain potential minimum. Consequently, a strong PL quenching was observed at high T, which is attributed to the evacuation of carriers from the QDs to non-radiative recombination centers through the ILs and barriers. Accordingly, it is confirmed that non-radiative

defects in the active region which may result from using the GaP and GaP/$In_{0.4}Ga_{0.6}P$ ILs can be compensated for QDs and the density of the InP QDs can be also increased.

4. Conclusion

Comparison of GaP and GaP/$In_{0.4}Ga_{0.6}P$ ILs indicates that not only the size and density can change, which leads to the improvement of optical properties of InP QDs. As a result, when the GaP and GaP/$In_{0.4}Ga_{0.6}P$ ILs were employed, the size of the QDs was reduced and the effective density of QDs was increased. A change of dot size was also led to a blueshift of the PL peak. The bimodal size distribution was overcome due to insertion of GaP and GaP/$In_{0.4}Ga_{0.6}P$ layers. The best compromise between the structural and optical properties is observed for a GaP/$In_{0.4}Ga_{0.6}P$ IL in comparison with a GaP IL. The GaP and GaP/$In_{0.4}Ga_{0.6}P$ ILs can also give the opportunity to "tune" the luminescence wavelength by altering the islands size.

Acknowledgements

The author wishes to thank ASEAN University Network/Southeast Asia Engineering Education Development Network (AUN/SEED-Net), the Higher Education Research Promotion and National Research University Project of Thailand, Office of the Higher Education Commission (EN264A), Integrated Innovation Academic Center: IIAC Chulalongkorn University Centenary Academic Development Project (CU-Energy/CU56-EN02), Nanotechnology Center of Thailand (Nanotech), Thailand Research Fund (TRF; DPG5380002), Chulalongkorn University, and the University of Tokyo for the support of this work.

References

[1] U. K. Mishra, J. B. Shealy, Sixth International Conference on InP and Related Materials, 1994, p. 14.
[2] N.M. Margalit, J. Piprek, S. Zhang, D.I. Babic, K. Streubel, P.P. Mirin, J.R. Wesselmann, J.E. Bowers, E.L. Hu, IEEE J. Sel. Top. Quantum Electron. 3 (1997) 359.
[3] L. Goldstein, C. Fortin, C. Starck, A. Plais, J. Jacquet, T. Boucart, A. Roche, C. Poussou, Electron. Lett. 34 (1998) 268.
[4] R. Szweda, III-Vs Review 13 (2000) 55.
[5] A. Mills, III-Vs Review 18 (2005) 27.
[6] M. Cooke, III-Vs Review 19 (2006) 23.
[7] D.Y.C. Lie, K.L. Wang, in: H.S. Nalwa (Ed.), Handbook of Advanced Electronic and Photonic Devices and Materials, Academic Press, San Diego, 2000, pp. 1–69. Chapter 1.
[8] D.Y.C. Lie, K.L. Wang, in: R. Willardson, E. Weber (Eds.), Semiconductors and Semimetals, Academic Press, San Diego, 2001, pp. 151–197. Chapter 4.
[9] X.B. Zhang, R.D. Heller, M.S. Noh, R.D. Dupuis, G. Walter Jr., N. Holonyak, Appl. Phys. Lett. 83 (2003) 1349.
[10] G. Walter, N. Holonyak Jr., J.H. Ryou, R.D. Dupuis, Appl. Phys. Lett. 79 (2001) 3215.
[11] G. Walter, N. Holonyak Jr., R.D. Heller, R.D. Dupuis, Appl. Phys. Lett. 81 (2002) 4604.
[12] N. Carlsson, W. Seifert, A. Petersson, P. Castrillo, M.E. Pistol, L. Samuelson, Appl. Phys. Lett. 65 (1994) 3093.
[13] N. Carlsson, K. Georgsson, L. Montelius, L. Samuelson, W. Seofert, R. Wallenberg, J. Cryst. Growth 156 (1995) 23.
[14] M.K. Zundel, P. Specht, K. Eberl, N.Y. Jin-Phillipp, F. Phillipp, Appl. Phys. Lett. 71 (1997) 2972.
[15] N. Carlsson, K. Georgsson, M. Montelius, L. Samuelson, W. Seifert, R. Wallenberg, J. Cryst. Growth 156 (1–2) (1995) 23–29.
[16] L.R. Wallenberg, K. Georgsson, W. Seifert, N. Carlsson, J. Lindahl, L. Samuelson, Phys. Status Solidi A 150 (1995) 479–487.
[17] H.-W. Ren, M. Sugisaki, J.-S. Lee, S. Sugou, Y. Masumoto, Jpn. J. Appl. Phys. 38 (Part1(1B)) (1999) 507–510.
[18] N. Carlsson, K. Georgsson, L. Montelius, L. Samuelson, W. Seifert, R. Wallenberg, J. Cryst. Growth 156 (1995) 23–29.
[19] W. Seifert, N. Carlsson, J. Johansson, M.E. Pistol, L. Samuelson, J. Cryst. Growth 170 (1997) 39–46.
[20] N. Chit Swe, O. Tangmattajittakul, S. Suraprapapich, P. Changmoang, S. Thainoi, C. Wissawinthanon, S. Kanjanachuchai, S. Ratanathammaphan, S. Panyakeow, J. Vac. Sci. Technol. B 26 (2008) 1100.
[21] P.R.C. Kent, L.W. Hart Gus, A. Zunger, Appl. Phys. Lett. 81 (2002) 4377.
[22] C.H. Roh, H.J. Song, D.H. Kim, J.S. Park, Y.S. Choi, H. Kim, C.K. Hahn, J. Appl. Phys. 101 (2007) 064320.
[23] L. Brusafemi, S. Sanguinetti, E. Grill, M. Guzzi, A. Bignazzi, F. Bogani, L. Carraresi, M. Colocci, Appl. Phys. Lett. 69 (1996) 3354.